

Phase effects in neutrino conversions during a supernova shock wave

Basudeb Dasgupta and Amold Bighe

Tata Institute of Fundamental Research, Homi Bhabha Road, Mumbai 400005, India

Abstract.

Neutrinos escaping from a core collapse supernova a few seconds after bounce pass through the shock wave, where they may encounter one or more resonances corresponding to m_{atm}^2 . The neutrino mass eigenstates in matter stay coherent between these multiple resonances, giving rise to oscillations in the survival probabilities of neutrino species. We point out these novel 'phase effects', and provide an analytic approximation to them that relates the density profile of the shock wave to the oscillation pattern. The phase effects can be strong if the multiple resonances encountered by neutrinos are semi-adiabatic, which typically happens for $10^5 < \sin^2 \theta_{13} < 10^3$. These effects would manifest themselves in oscillations in the observed neutrino spectra for certain neutrino mixing scenarios. The time dependent neutrino spectra from a future galactic supernova can then be used to identify the neutrino mixing scenario as well as reconstruct the density profile in the region around the reverse shock.

PACS numbers: 14.60.Pq, 97.60.Bw

1. Introduction

The neutrino fluxes emitted from a core collapse supernova (SN) contain information about the primary fluxes produced inside the star, the neutrino mixing pattern as well as the matter densities that the neutrinos have passed through. The high statistics neutrino signal that one expects from a future galactic SN needs to be decoded in order to extract this information.

The neutrinos and antineutrinos produced inside the SN pass through the core, mantle and envelope of the progenitor star before escaping. They encounter matter densities ranging from nuclear densities deep inside the core all the way to vanishingly small densities in the interstellar space. Neutrino masses and mixing angles, and hence the extent of their flavour conversions, depend crucially on the density of surrounding matter, hence it is important to study these matter effects in detail.

The matter effects [1] give rise to MSW resonances [2] when the matter density corresponds to

$$R = m^2 \cos 2 \theta_M = \left(\frac{p}{2G_F Y_e E} \right) : \quad (1)$$

Here Y_e is the electron fraction, M_N the average nucleon mass, and the plus and minus signs correspond to neutrinos and antineutrinos respectively. For neutrinos of energy E , resonances are possible at two densities, the H resonance corresponding to $(m^2; +)$ ($m_{\text{atm}}^2; 13$) and the L resonance corresponding to $(m^2; -)$ ($m^2; 12$). The energies of SN neutrinos are typically in the range 5–50 MeV. For these energies, the H resonance takes place around $H \approx 500\text{--}5000$ g/cc. It occurs in neutrinos for normal hierarchy and in antineutrinos for inverted hierarchy. The L resonance that takes place around $L \approx 20\text{--}200$ g/cc always occurs in neutrinos.

The adiabaticities at the H and L resonances determine the net neutrino conversion probabilities. The L resonance is always adiabatic, given the values of $m^2; 12$ and the typical density profile of the progenitor star around L . The adiabaticity at the H resonance is very sensitive to the value of 13 and the density profile of the star in the resonance region. Indeed the neutrino conversion rates are crucially dependent on the value of 13 , and whether the H resonance is in neutrinos or antineutrinos. The SN signal can therefore be an extremely sensitive probe of 13 and whether the mass hierarchy is normal or inverted [3].

In addition to divulging the neutrino mixing scenario, SN neutrino fluxes can also allow us to have a peek at the propagation of the shock wave while it is still inside the mantle of the star. The violent density fluctuations caused by the SN shock wave can change the adiabaticity at H resonance in a time dependent manner, thus leaving their imprint on the time dependent neutrino spectra [4, 5, 6, 7]. In particular, the observations of the time dependent neutrino spectra can confirm the presence of forward as well as reverse shock wave through the "double dip" feature [8], and in addition can track the positions of the shocks as they pass through the H resonance region. The feasibility of such a tracking at a water Cherenkov detector has been explored in [9].

Our understanding of the SN explosion mechanism is still unsatisfactory [10, 11], which makes it very important to extract as much information about the shock wave as possible. In this paper, we demonstrate how the neutrinos that pass through the shock wave near the H resonance carry information about the density profile of the shock wave. In addition to making the H resonance temporarily nonadiabatic, the shock wave also forces the neutrinos to encounter multiple H resonances. The relative phases that the neutrino mass eigenstates gain between two or more of such H resonances manifest themselves as oscillations in the neutrino flavour conversion probabilities as a function of the neutrino energy. These oscillations are related to the shock wave density profile.

Most of the analyses of SN neutrino conversions till now calculate the probabilities of conversions between neutrino mass eigenstates in matter in the resonance regions, and combine the results at different resonances, assuming them to be independent. This includes the implicit assumption that the information on the relative phase between the neutrino mass eigenstates is lost between successive resonances. For neutrinos that undergo a single H and a single L resonance, this is a valid assumption since the two resonance regions are well separated. However, when the neutrinos encounter multiple H resonances that are close to each other, coherence between the neutrino mass eigenstates is maintained, and one has to compute the amplitudes of neutrino flavour conversions at the resonances, keeping track of the relative phases. This gives rise to the novel 'phase effects' that we point out.

If the multiple resonances are semi-adiabatic, the phase effects will be strong and the observation of the oscillation pattern present in the observed neutrino spectra can help us infer about the density profile of the shock wave, which in turn can provide us important clues about the shock wave propagation and the SN explosion.

The paper is organised as follows. In Sec. 2, we give an analytic approximation for calculating the neutrino conversion probability when multiple H resonances are taken into account in a two-neutrino framework. The results of this section are general and can be applied to any situation where multiple resonances are involved. In Sec. 3, we apply the results to the case of a SN shock wave, where the third neutrino and the L resonance are included. We show the neutrino conversion probabilities obtained by using a realistic shock wave profile and demonstrate how the oscillation pattern can help us reconstruct features of the shock wave. Sec. 4 concludes.

2. Phase effects from multiple resonances

In this section, we calculate the survival probability of ν_e when they pass through multiple resonances, keeping track of the relative phases between the mass eigenstates. The calculations are performed in the 2- framework. The results are readily extended to the 3- framework in the case of a SN shock wave, as will be shown in Sec. 3. Although all the arguments in this section are given for neutrinos, they are valid for antineutrinos just by changing the signs of the matter potential $A(x)$ and the mass squared difference m^2 .

2.1. Survival probability of e^- for a small mixing angle

The relevant mixing angle at the resonance H is $\theta_{13} = 13^\circ$, on which we currently have a strong bound: $\sin^2 \theta_{13} < 0.05$ [12]. Therefore, we try to solve the problem using small angle approximation. We follow the notation and framework outlined in [13] and work in the flavour basis.

Let ψ be the relevant linear combination of ν_e and ν_μ . When neutrinos pass through matter, their propagation is described by the Schrödinger equation

$$i \frac{d}{dx} \psi = \frac{1}{4E} [A(x) - m^2 \cos 2\theta_{13} \sin 2\theta_{13} \bar{A}(x) + m^2 \cos 2\theta_{13}] \psi : \quad (2)$$

where $A(x) = 2E V(x) = \frac{p}{2} \frac{1}{2G_F Y_e} E = M_N$. These two coupled first order equations give rise to the second order equation

$$\frac{d^2}{dx^2} \psi = (-\frac{1}{4E} + i \frac{\partial}{\partial x}) \psi = -\frac{m^2}{4E} \psi : \quad (3)$$

where

$$\frac{\partial}{\partial x} \psi = \frac{1}{4E} [A(x) - m^2 \cos 2\theta_{13}] \psi = -\frac{m^2}{4E} \sin 2\theta_{13} \psi : \quad (4)$$

and prime (\prime) denotes derivative with respect to x . In order to find the survival probability of ν_e , we solve for the ψ wavefunction with the initial conditions $\psi_e(0) = 1$, $\psi_e'(0) = 0$. These conditions are equivalent to

$$\psi_e(0) = 1 ; \quad i \frac{d}{dx} \psi_e(0) = 0 : \quad (5)$$

The "logarithmic perturbation" approximation [13] solves the differential equation (3) for small mixing angles by choosing

$$g = 1 - \cos 2\theta_{13} : \quad (6)$$

as the small expansion parameter. Denoting

$$\psi_e = e^{S(x)} ; \quad \text{with} \quad S^0(x) = c_0(x) + g c_1(x) + O(g^2) : \quad (7)$$

so that

$$\psi_e(x) = \exp \left[\int_0^x dx_1 c_0(x_1) + g \int_0^x dx_1 c_1(x_1) + O(g^2) \right] : \quad (8)$$

the solution becomes

$$\begin{aligned} \psi_e(x) = & \exp \left[\frac{iQ(x)}{2} - g \frac{im^2 x}{4E} \right. \\ & \left. + g \frac{(m^2)^2}{2(2E)^2} \int_0^x dx_1 e^{iQ(x_1)} \int_0^{x_1} dx_2 e^{iQ(x_2)} + O(g^2) \right] : \quad (9) \end{aligned}$$

Here we have defined the "accumulated phase"

$$Q(x) = \frac{1}{2E} \int_0^x dx_1 A(x_1) - \frac{m^2}{4E} x : \quad (10)$$

The survival probability $P_{ee}(x) = P_0(e \rightarrow e)$ at $x = X$ then becomes

$$P_{ee}(X) = \exp \left(-\frac{g^2 (m^2)^2}{2(2E)^2} \int_0^X dx_1 e^{iQ(x_1)} A + O(g^2) \right) : \quad (11)$$

The integral in the above expression can be evaluated using the stationary phase approximation. The integral oscillates rapidly unless $Q^0(x) = 0$. So the entire contribution to the integral can be taken to be from the saddle point x_s , which is the point where $Q^0(x_s) = 0$, i.e.

$$A(x_s) = m^2 : \quad (12)$$

Note that this is also the resonance point in the small angle limit.

For a monotonic density profile, there is only one saddle point x_s and the survival probability is

$$P_{ee} = \exp \left(-\frac{g^2 (m^2)^2}{2E A^0(x_s)} \right) : \quad (13)$$

which agrees with the Landau-Zener jump probability [14, 15] in the limit of small mixing angle, and hence small g , even when $P_{ee} = 1$.

For a non-monotonic density profile, neutrinos can experience more than one resonance at the same density but at different positions. In that case $Q^0(x) = 0$ at more than one point. If the resonances are sufficiently far apart, the contributions from each of them may be added independently of each other. Their total contribution to the integral in (11) is

$$\int_0^X dx e^{iQ(x)} = \sum_i \int_{x_i}^{x_s} e^{iQ(x)} + \sum_{i \neq s} \int_{x_s}^X e^{iQ(x)} = \frac{4 \pi E}{A^0(x_s)} : \quad (14)$$

where i runs over all the saddle points. Note that $= 4$ if $A^0(x_s) < 0$ and $= 3 = 4$ if $A^0(x_s) > 0$. The probability calculated using (11) now has terms which depend on the differences between the integrated phases

$$\sum_{ij} Q(x_j) - Q(x_i) + \int_j^i = \sum_{x_i}^{x_j} \frac{1}{2E} \int_{x_i}^{x_j} A(x) m^2 dx : \quad (15)$$

In general,

$$P_{ee}(X) = \exp \left(-\frac{g^2}{4} \sum_i^0 \int_{x_i}^X a_i^2 + 2 \sum_{i < j}^X a_i a_j \cos \int_{ij} A \right) + O(g^2) : \quad (16)$$

where

$$a_i = \frac{(m^2)^2}{2E A^0(x_i)} : \quad (17)$$

For example, when there are only two saddle points the survival probability is given by

$$P_{ee} = \exp(-g_1^2) \exp(-g_2^2) \exp(-2g_1 a_2 \cos \theta_{12}) : \quad (18)$$

The first two factors in (18) are the individual Landau-Zener jump probabilities for the two level crossings. The last factor gives rise to oscillations in P_{ee} as a function of energy.

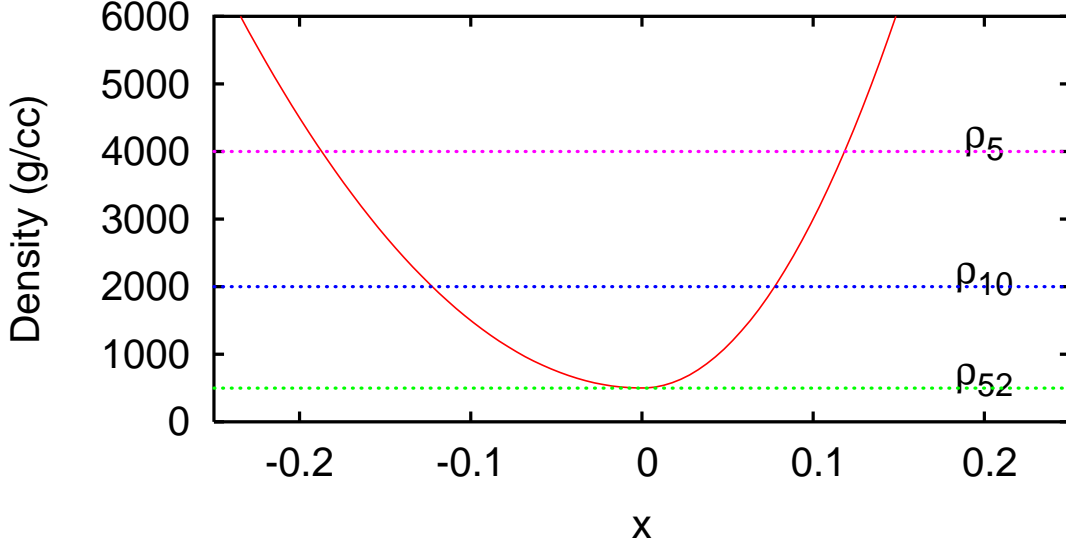


Figure 1. Density profile (19) with $a = 500 \text{ g/cc}$, $b_1 = 10^5 \text{ g/cc} = (10^8 \text{ cm})^2$ and $b_2 = 2.5 \cdot 10^5 \text{ g/cc} = (10^8 \text{ cm})^2$. The horizontal lines on the graph are the resonance densities for various energies (5, 10, 52 M eV). Notice how the saddle points come closer for larger energies till $E = E_{\text{R max}} = 52 \text{ M eV}$, after which there is no resonance.

The oscillation pattern has its maxima at $\theta_{12} = (2n + 1) \pi$ and minima at $\theta_{12} = 2n \pi$ where n is an integer.

We illustrate the validity and limitations of the small angle approximation with a toy density profile

$$\rho(x) = \begin{cases} a + b_1 x^2 & (x < 0) \\ a + b_2 x^2 & (x > 0) \end{cases}; \quad (19)$$

as shown in Figure 1. Neutrinos are produced at $x \neq 0$ and we calculate P_{ee} at $x \neq 0$. We also show the positions of resonance points for various energies.

Figure 2 shows the survival probability P_{ee} as a function of energy, both the exact numerical result and the result of our analytic approximation for small angles. It can be seen that at such small angles ($\theta = 0.02 \text{ rad} \approx 1.1^\circ$), the approximation works extremely well.

Note that the amplitude of the oscillations is comparable to the deviation of the average survival probability from unity. That is, the oscillation effect is not a small effect. Indeed, the oscillation term is of the same order as the averaged effect, as can be seen from (18). Figure 2 also shows the average value of P_{ee} that one would have obtained if one naively combined the jump probabilities at the two resonances. Our analysis gives additional oscillations in the survival probability as a function of neutrino energy about this average value. This novel effect is what we call as the 'phase effect,' and is clearly significant as can be seen from the figure. An important feature of the oscillations is that the 'wavelengths,' i.e. the distances between the consecutive maxima and minima, are larger at larger E .

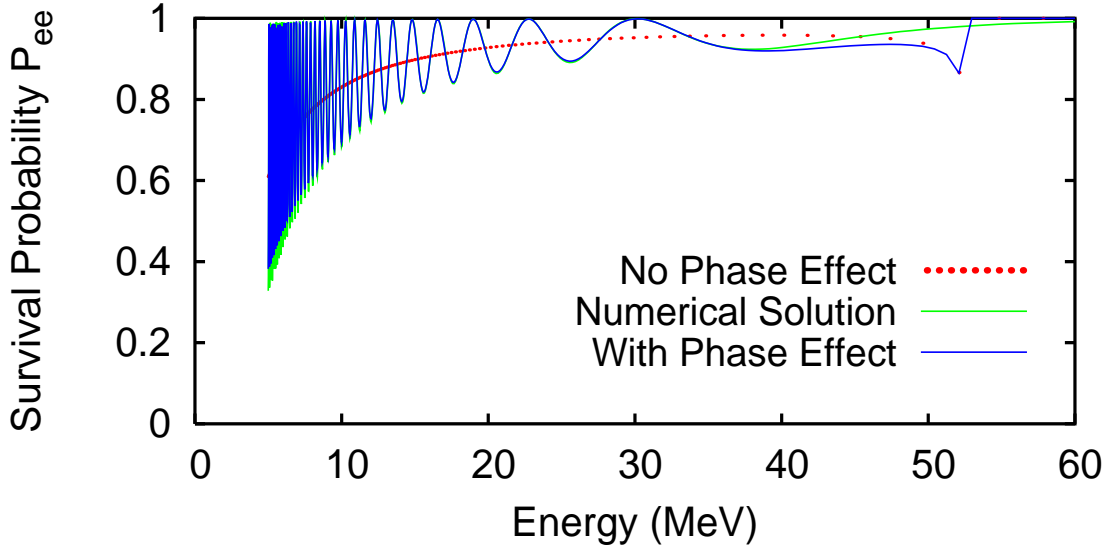


Figure 2. Survival probability P_{ee} as a function of energy for $\theta = 0.02$ rad. The green (light) curve is the numerically evaluated exact result. The blue (dark) curve is our solution with small angle approximation including the phase effects. The red (dotted) curve is the approximate solution if the phase effects are neglected. Notice that our approximate solution is valid only upto $E = E_R(\text{max})$.

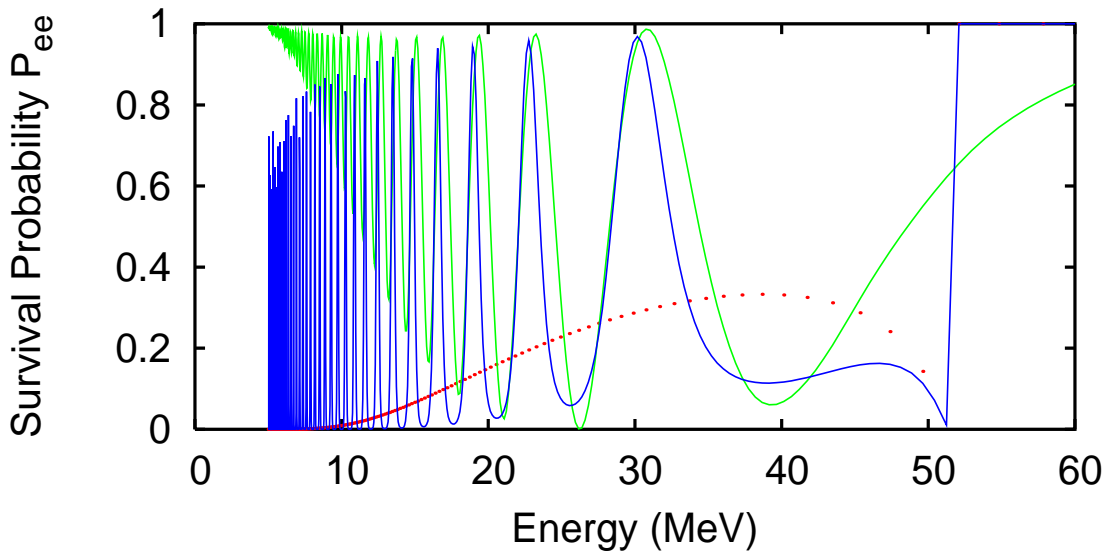


Figure 3. Survival probability P_{ee} as a function of energy for $\theta = 0.1$ rad. The convention for the lines is the same as that used in figure 2.

The resonances start overlapping at $E = E_{R(\text{max})}$ (figure 1), which is where our approximation starts breaking down, as can be seen in figure 2. For $E > E_{R(\text{max})}$, the neutrinos no longer encounter a strict resonance, and our approximation gives $P_{ee} = 0$ identically. However, the resonances have finite widths which may affect the conversion probabilities of neutrinos with $E = E_{R(\text{max})}$. The sharp jump observed in figure 2 at $E = 52 \text{ MeV}$ is therefore not a real effect, but a limitation of our technique.

The small angle approximation starts failing for larger angles and lower energies. Figure 3 shows that the amplitude at low energies is not calculated correctly for $\theta = 0.1$ rad = 5.7°. However, note that the positions of maxima and minima of P_{ee} are still predicted to a good accuracy. We shall argue in the next subsection that these can be computed accurately for the whole allowed range of θ , given the non-monotonic density profile between the two resonances.

2.2. The oscillations in $P_{ee}(E)$

Let us consider a density profile with a "dip" as in the toy model in the previous section. A neutrino with energy E encounters two resonances R_1 and R_2 at $x = x_1$ and $x = x_2$ respectively, so that

$$R(x) = (x_2) : \quad (20)$$

We assume Y_e to be a constant throughout the region of interest. We also assume that the propagation of neutrino mass eigenstates is adiabatic everywhere except in the resonance regions $(x_1^-; x_1^+)$ and $(x_2^-; x_2^+)$ around the resonance points x_1 and x_2 respectively. In the limit of small angles, the widths of the resonances are small:

$$\tan 2\theta : \quad (21)$$

Therefore, $x_1 \approx x_{1+}$ and $x_2 \approx x_{2+}$. We shall work in this approximation, and shall use the notation x_i only for the sake of clarity wherever needed.

At $x = x_1$, the density $R(x) \approx R$, so that the heavier mass eigenstate h is approximately equal to the flavour eigenstate e . Let us start with e as the initial state:

$$e(x = x_1) \approx h : \quad (22)$$

The mass eigenstate h propagates adiabatically till it reaches the resonance region $x = x_1$:

$$e(x_1) \approx h : \quad (23)$$

While passing through the resonance, unless the resonance is completely adiabatic, the state becomes a linear combination of h and l , the lighter mass eigenstate. Note that the phases of h and l can be defined to make their relative phase vanish at $x = x_{1+}$.

$$e(x_{1+}) = \cos \theta_{1h} + \sin \theta_{1l} ; \quad (24)$$

where $P_1 = \sin^2 \theta_{1l}$ is the "jump probability" at R_1 if it were an isolated resonance.

The two mass eigenstates $_{\text{H}}$ and $_{\text{L}}$ propagate to the other resonance R_2 , gaining a relative phase in the process (the overall phase of the state is irrelevant):

$$_{\text{e}}(x_2) = \cos_{1\text{H}} + \sin_{1\text{H}} \exp i \int_{x_1}^{x_2} \frac{m^2}{2E} dx \quad \text{L} ; \quad (25)$$

where m^2 is the mass squared difference between $_{\text{H}}$ and $_{\text{L}}$ in matter:

$$m^2(x;E) = \frac{[m^2 \cos^2 2E V(x)^2 + (m^2 \sin^2 2)^2]}{q} ; \quad (26)$$

The effect of the resonance R_2 may be parameterised in general as

$$\begin{aligned} {}_{\text{H}}(x_{2+}) &= \cos_{2\text{H}} \sin_{2\text{H}} e^{i\theta} & {}_{\text{H}}(x_2) &= \cos_{2\text{H}} \sin_{2\text{H}} e^{i\theta} \\ {}_{\text{L}}(x_{2+}) &= \sin_{2\text{L}} e^{i\theta} & {}_{\text{L}}(x_2) &= \cos_{2\text{L}} \sin_{2\text{L}} e^{i\theta} \end{aligned} ; \quad (27)$$

where $P_2 = \sin^2_{2\text{H}}$ is the 'jump probability' at R_2 if it were an isolated resonance.

From (9), one can deduce that in the limit $x_2 \rightarrow x_{2+}$, we have $Q(x_{2+} - x_2)$

0. The state $_{\text{e}}(x_{2+})$ can then be written as

$$\begin{aligned} {}_{\text{e}}(x_{2+}) &= \cos_{2\text{H}} \cos_{1\text{H}} + \sin_{2\text{H}} \sin_{1\text{H}} \exp i \int_{x_1}^{x_2} \frac{m^2}{2E} dx & {}_{\text{H}} &= \cos_{2\text{H}} \cos_{1\text{H}} \\ &+ \cos_{2\text{L}} \sin_{1\text{H}} \exp i \int_{x_1}^{x_2} \frac{m^2}{2E} dx & {}_{\text{L}} &= \sin_{2\text{L}} \cos_{1\text{L}} \end{aligned} ; \quad (28)$$

For $x > x_{2+}$, the mass eigenstates travel independently and over sufficiently large distances, decohere from one another. At $x = x_2$, since $(x) \rightarrow R$, the heavier mass eigenstate $_{\text{H}}$ again coincides with $_{\text{e}}$ and we get the $_{\text{e}}$ survival probability as

$$P_{\text{ee}} = \cos_{2\text{H}} \cos_{1\text{H}} + \sin_{2\text{H}} \sin_{1\text{H}} \exp i \int_{x_1}^{x_2} \frac{m^2}{2E} dx \quad (29)$$

$$= \cos^2_{1\text{H}} \sin^2_{2\text{H}} + \sin^2_{1\text{H}} \sin^2_{2\text{H}} \exp i \int_{x_1}^{x_2} \frac{m^2}{4E} dx ; \quad (30)$$

If the phase information were lost, either due to decoherence or due to finite energy resolution of the detectors [16] the survival probability would have been

$$P_{\text{ee}}(\text{no phase}) = P_1 P_2 + (1 - P_1)(1 - P_2) = \cos^2_{1\text{H}} \cos^2_{2\text{H}} + \sin^2_{1\text{H}} \sin^2_{2\text{H}} ; \quad (31)$$

which matches with (30) when the $\sin^2(\theta)$ term is averaged out to 1/2.

The $\sin^2(\theta)$ term in (30) gives rise to the oscillations in $P_{\text{ee}}(E)$. If two consecutive maxima of P_{ee} are at energies E_1 and E_2 such that $E_1 > E_2$, then the condition

$$\int_{x_1(E_2)}^{x_2(E_2)} \frac{m^2(x;E_2)}{2E_2} dx = \int_{x_1(E_1)}^{x_2(E_1)} \frac{m^2(x;E_1)}{2E_1} dx = 2 \quad (32)$$

is satisfied. The quantity $(E_1 - E_2)$ is the 'wavelength' of the oscillations.

Note that $m^2(x;E)$ is equal to $\frac{1}{2} \int_{x_1}^x m^2 dx$ in the small angle limit. Moreover, this quantity is rather insensitive to θ in the allowed range of θ . Therefore, it is not a surprise that the predictions of the positions of maxima and minima in the small angle approximation (Sec. 2.1) are accurate and robust in the whole range $\theta < 13^\circ$.

Since θ is small, the left hand side of (32) is approximately equal to the area enclosed by the density profile (x) and the lines $x = E_1$ and $x = E_2$, scaled by $M_N = (\frac{1}{2} G_F Y_e)$. This observation is instrumental in reconstructing the density profile from the observed oscillation pattern, as we shall demonstrate in the next section.

3. Oscillations during the SN shock wave propagation

In this section, we apply the results in the last section to the neutrinos travelling through a supernova shock wave. Though we have to consider three-neutrino mixing in this case, the separation of H and L resonances [17] means that we can calculate the transition probabilities at these resonances separately. Each of these resonances can then be treated as an effective two-neutrino level crossing. The L resonance that takes place in neutrinos is always adiabatic [3], whereas the jump probability P_H between the two mass eigenstates at the H resonance is equal to P_{ee} as computed in the previous section. The survival probability of ν_e after passing through both the H and L resonances is

$$p = P_H \sin^2(\text{NH}); \quad p = \sin^2(\text{IH}) \quad (33)$$

where NH and IH stand for normal and inverted mass hierarchy respectively. Here θ is the solar mixing angle. Similarly, the survival probability of ν_e after passing through both the H and L resonances is

$$p = P_H \cos^2(\text{IH}); \quad p = \cos^2(\text{NH}) : \quad (34)$$

Clearly, since the phase effects appear through P_H , they will be visible only in ν_e for normal hierarchy and only in ν_e for inverted hierarchy.

In present and planned water Cherenkov [18] and scintillation [19] detectors, the main neutrino detection channel is the inverse beta decay reaction $\nu_e p \rightarrow e^- n$ that allows the reconstruction of ν_e energies. Therefore we consider only the ν_e spectrum in our analysis. However an analogous analysis can be easily performed in the neutrino channel for a detector able to measure the ν_μ spectrum, for example using liquid argon [20].

In order to illustrate the phase effects on p or p , we consider a typical snapshot of the density profile of a SN during a shock wave [8], as shown in figure 4. The forward shock F and the reverse shock R are sharp density discontinuities, the density change of a factor of two or more taking place over a distance of much less than a km. The density variation in the "contact discontinuity" C, which is the transition region between the shock-accelerated and neutrino-heated SN ejecta, takes place more slowly, over a distance of more than 100 km [8]. The mass accretion region A behind the forward shock wave, and the low density bubble B have gradually changing densities. The region T is the tail of the shock wave.

The neutrinos, while passing through these regions, may undergo multiple level crossings. The extent of flavour conversion in each region will depend on the value of θ_{13} and the steepness of the density profile in that region. It is found that for $\theta_{13} = 0.01$ rad or higher, the density variations in the mass accretion region A, the low density bubble B and the contact discontinuity C are too gradual for any non-adiabaticity. We therefore concentrate on the forward shock F, the reverse shock R and the tail T.

Figure 5 shows the value of p as a function of energy for $\theta_{13} = 0.02$ rad and $\theta_{23} = 1.1$. The rapid oscillations correspond to the relative phase $\phi_{RF} - \phi_{TF}$ that is accumulated by the mass eigenstates between resonance regions R and F (T and F). Such high

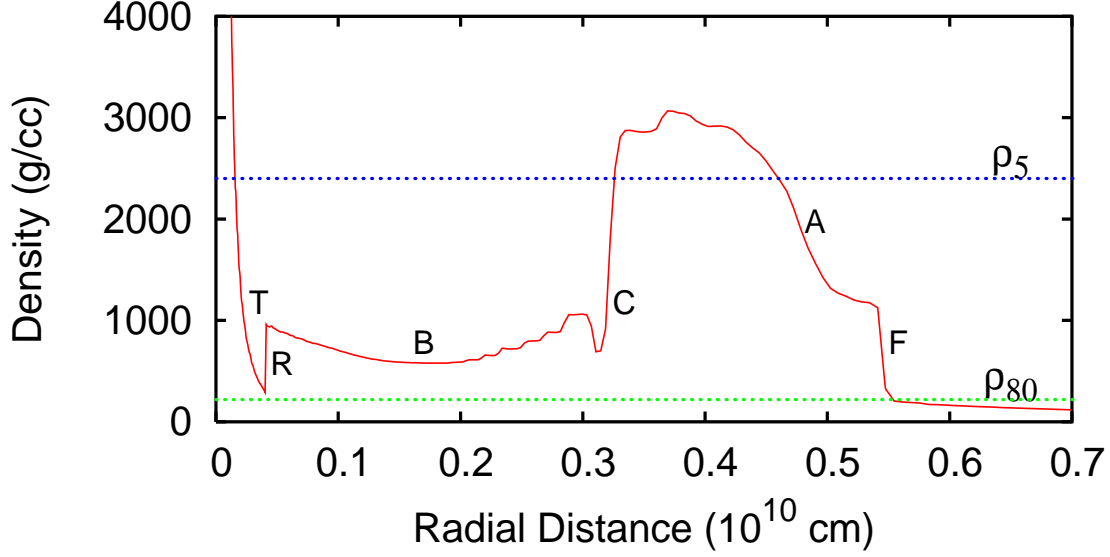


Figure 4. Snapshot of a shock wave density profile at $t = 5$ sec. The resonance densities for $E = 5$ and 80 MeV are also shown.

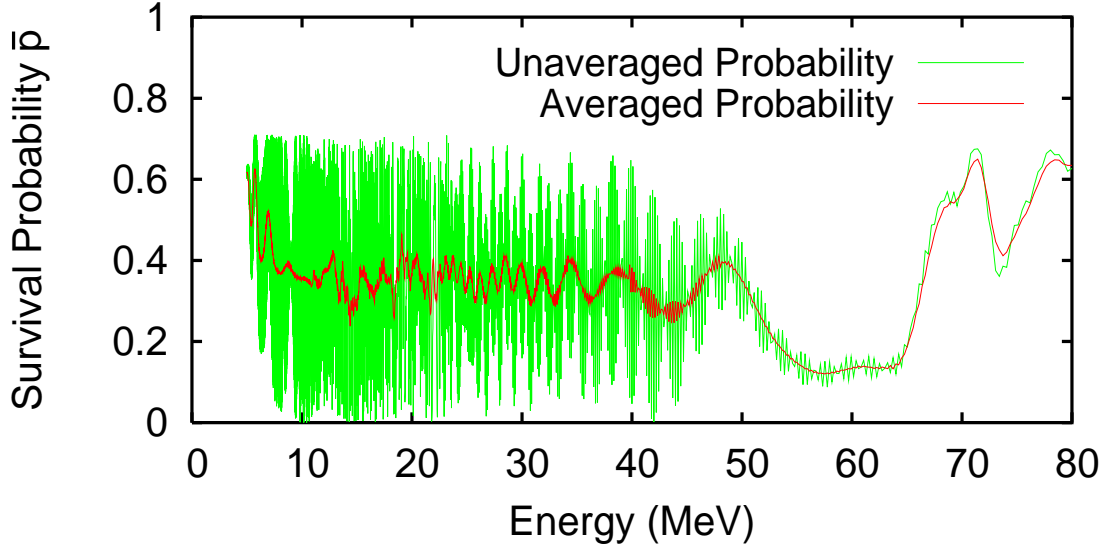


Figure 5. Survival probability p of ν_e for inverted hierarchy with the density profile in figure 4. The "averaged probability" is obtained by taking a running average over the energy range corresponding to the typical energy resolution of a scintillation detector.

frequency oscillations are virtually impossible to observe, given the practical limits on the energy resolutions of neutrino detectors.

We average out these high frequency oscillations by taking a "running average" over the energy range corresponding to the typical energy resolution of a scintillation detector. The low frequency oscillations that survive are found to correspond to the

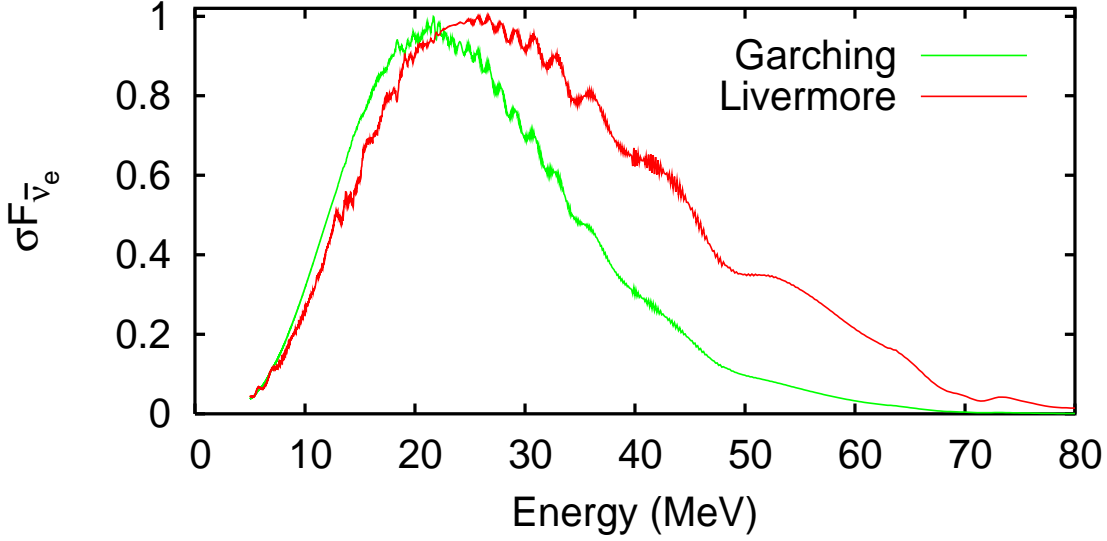


Figure 6. Oscillations in the "observed fluxes" F_ν for the Garching model (green/light) and the Livermore model (red/dark). The fluxes have been normalized such that their peak values are unity. We use the averaged survival probability as shown in figure 5.

relative phase τ_R accumulated by the mass eigenstates between resonances in regions T and R. Since these two resonances are closer compared to the resonance pairs R-F or T-F, the frequency of oscillations is smaller. The same oscillation pattern is observed if the survival probability is computed by assuming that the resonance in region F is completely adiabatic, which means that the pattern is indeed due to the levelcrossings in regions T and R. These low frequency oscillations may be observable at the neutrino detectors.

The second dip observed at $E = 70\text{--}80\text{ MeV}$ is a part of the "double dip" feature pointed out in [8] that appears due to the presence of both the forward as well as the reverse shock.

In order to demonstrate the oscillation effects in the observed ν_e flux at a neutrino detector, we plot in figure 6 the quantity

$$\langle E \rangle F_e = \langle E \rangle [p F_e^0 + (1 - p) F_x^0] = \langle E \rangle [F_x^0 + p (F_e^0 - F_x^0)] \quad (35)$$

where we take the cross section $\langle E \rangle / E^2$. The primary fluxes of ν_e and ν_x , denoted by F_e^0 and F_x^0 respectively, are parametrized by

$$F_i^0 = \frac{E_0}{E} \frac{(1 + \beta)^{1+\gamma}}{(1 + \beta)^{\gamma}} \exp \left(-\gamma \frac{E}{E_0} \right) \quad (36)$$

For illustration, we choose two models of neutrino flux, the Garching model [21] that uses the parameters

$$\nu_e = \nu_x = 3; E_0(\nu_e) = 15\text{ MeV}; E_0(\nu_x) = 18\text{ MeV}; \gamma_0(\nu_e) = \gamma_0(\nu_x) = 0.8;$$

and the Livermore model [22] that uses

$$e = x = 3; E_0(e) = 15 \text{ MeV}; E_0(x) = 24 \text{ MeV}; \alpha(e) = \alpha(x) = 1.6;$$

The phase effects are clearly present in both the scenarios. Moreover, the local minima of the Garching model are observed to be at the same energies as the local minima of the Livermore model. This out-of-phase nature of oscillations is due to the fact that in the energy range of interest, the quantity $(F_e^0 - F_x^0)$ in (35) is negative for the Garching model and positive for the Livermore model.

The observation of the oscillation pattern in e spectrum reveals the following:

It seems that the mass hierarchy is inverted (if the oscillations were in e spectrum, the hierarchy would have been normal)

The time interval during which the oscillations appear tells the times at which the shock wave was present in the region of densities 500{5000 g/cc.

The mixing angle θ_{13} is nonzero. Indeed, $\sin^2 \theta_{13} > 10^{-5}$ for the oscillations to be observable.

If θ_{13} has already been measured at reactor experiments, one can obtain constraints on the slopes of the features within the shock wave profile. In particular, even though the forward and the reverse shock may be taken to be almost density discontinuities, the slope of the tail T needs to be steep enough to ensure that the resonance there is semi-adiabatic.

With $m^2 = m_{\text{atm}}^2$ known and θ_{13} small, the distance between consecutive maxima or minima of the oscillation pattern depends only on the density profile immediately behind the reverse shock.

The density profile immediately behind the reverse shock may be partially reconstructed through the following procedure. Figure 7(a) shows a zoomed-in view of the plot of F_e as a function of energy. Let E_k be the energies corresponding to the local minima, with increasing k corresponding to decreasing energies. As pointed out in Sec. 2.2, the area of the region enclosed by the density profile between the densities E_k and E_{k+1} is

$$A = 2 \frac{M_N}{2G_F Y_e}; \quad (37)$$

The distance between the reverse shock R and the tail T in the region $E_k < E < E_{k+1}$ is then

$$r_k = A = (E_{k+1} - E_k); \quad (38)$$

This procedure may be repeated to estimate the T-R distance for all the maxima that can be identified. Since the reverse shock may be approximated well by a density discontinuity, this procedure can be used to reconstruct the density profile in the T region. Figure 7(b) indicates this procedure in a visual form. The resolution of $r(\cdot)$ may be increased by using the local minima in addition to the maxima, taking into

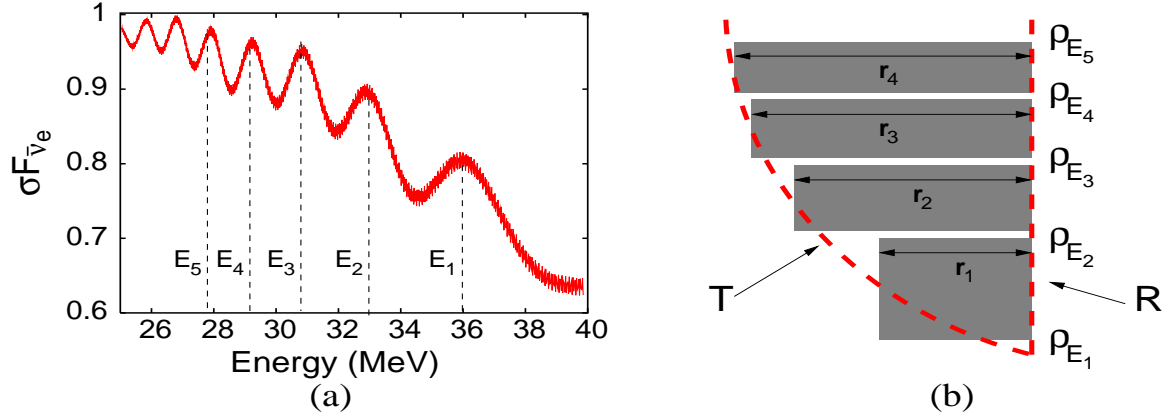


Figure 7. Reconstructing the density profile of the tail T from the oscillations in the observed flux shown in (a). The area of each rectangle in (b) is equal to A .

account that the phase between a minimum and the next maximum is half the phase between two consecutive maxima or minima.

This procedure for reconstructing the tail of the shock wave is somewhat crude, and the information obtained is only on the density profile along the line of sight. However, it is the only way we know as of now that can tell us about the density profile deep inside the SN directly from the data. Moreover, note that this procedure is not affected by the uncertainties in the primary fluxes, since the positions of the maxima and minima are independent of the primary fluxes.

The factors limiting the identification of the local maximum in the neutrino spectra are statistical fluctuations and the finite energy resolutions of the detector. Both of these have not been taken into account in our analysis above. Since the shock wave propagates with time to lower densities, the neutrino signal needs to be binned in time and only those neutrinos within a small time range can be used to look for the maxima and minima at that time. While this allows us to determine the shock wave features at many different times, the number of events available in each time bin also decreases.

The energy resolution of a water Cherenkov detector is typically equal to $E_{\text{CH}} (\text{MeV}) = 1.6 E (10 \text{MeV})$, which is also a function of the phototube coverage. For a scintillation detector, the resolution is much better, $E_{\text{SC}} (\text{MeV}) = 0.2 E (10 \text{MeV})$. So one would expect that only a very few local extrema will be practically observable at a water Cherenkov detector, whereas many more should be observable at a scintillation detector. For a 32 kton scintillation detector like LENA [19], the main limitation is expected to be the statistical fluctuations, whereas for a megaton water Cherenkov like Hyper-Kamiokande [18], the limiting factor would be its energy resolution.

4. Summary and conclusions

When the neutrinos escaping from the core of a core collapse SN pass through the shock wave, they may encounter multiple resonances corresponding to m_{atm}^2 and $_{13}$, when the shock wave is in the regions with densities around $500\{5000$ g/cc. We have shown that this gives rise to oscillations in the observed neutrino fluxes, and calculated the survival probability of neutrinos as a function of energy. We show an analytic approximation for small mixing angles and show that the oscillations are a significant effect: they are of the same order as the non-oscillating terms.

The local maxima and minima in the observed spectra of ν_e or $\bar{\nu}_e$ are determined by the relative phase accumulated by the neutrino mass eigenstates between the multiple resonances. The positions of these extrema as a function of time can reveal information on the propagation of the shock wave: its location as well as the density variation present in it. In particular, the density profile immediately behind the reverse shock can be partially reconstructed independently of the models of primary neutrino fluxes. In addition, the mere observation of oscillations can also determine the neutrino mass hierarchy and give a lower bound on $_{13}$.

The feasibility of determination of the positions of local extrema at specific detectors and the constraints one can get on the shock wave as well as neutrino mixing parameters will be dealt with in a future detailed study.

The phase effects pointed out here result from the interference between two or more MSW resonances. This novel phenomenon is not restricted to the SN alone, but may occur whenever neutrinos pass through nonmonotonic matter densities. It should be emphasized that this phenomenon is the only way we know of obtaining information on the density variation deep inside the SN shock wave directly from the data, without relying on any SN model.

The neutrino signal may show oscillations even when the neutrinos travel through the earth before reaching the detector [23, 24]. However, the Earth effect oscillations have a frequency in "inverse energy" which is constant in time and depends only on the distance travelled by the neutrinos inside the Earth. Therefore, the oscillations from these two sources can in principle be separated.

The typical values of $_{13}$ that gives rise to the oscillation features are in the "transition region" of the neutrino mixing parameter space [3], that is significant in range ($10^{-5} < \sin^2 _{13} < 10^{-3}$), but is usually neglected in the SN analysis for simplicity. In the light of the distinctive features like the ones pointed out in this paper, this region deserves detailed investigation.

Acknowledgments

We would like to thank R. Buras and L. Scheck for help in understanding features of the shock wave. AD would like to thank the Max Planck Institute for Physics for hospitality during the initial part of the work. We would like to especially thank B.

Bhattacharya for useful discussions, and H.-Th. Janka, G. G. Raelt and R. Tom as for comments on the manuscript. This work was partly supported through the Partner Group program between the Max Planck Institute for Physics and Tata Institute of Fundamental Research.

References

- [1] L.W. Ol'enstein, *Neutrino oscillations in matter*, Phys. Rev. D 17 (1978) 2369.
- [2] S.P. Mikheev and A.Yu. Smirnov, *Resonance enhancement of oscillations in matter and solar neutrino spectroscopy*, Sov. J. Nucl. Phys. 42 (1985) 913 [Yad. Fiz. 42 (1985) 1441].
- [3] A.S. Dighe and A.Yu. Smirnov, *Identifying the neutrino mass spectrum from the neutrino burst from a supernova*, Phys. Rev. D 62 (2000) 033007 [hep-ph/9907423].
- [4] R.C. Schirato and G.M. Fuller, *Connection between supernova shocks, flavor transformation, and the neutrino signal*, astro-ph/0205390.
- [5] K.Takahashi, K.Sato, H.E.Dalhed and J.R.Wilson, *Shock propagation and neutrino oscillation in supernova*, Astropart. Phys. 20 (2003) 189 [astro-ph/0212195].
- [6] C.Lunardini and A.Yu. Smirnov, *Probing the neutrino mass hierarchy and the 13-mixing with supernovae*, JCAP 0306 (2003) 009 [hep-ph/0302033].
- [7] G.L. Fogli, E.Lisi, D.Montanino and A.Mirizzi, *Analysis of energy- and time-dependence of supernova shock effects on neutrino crossing probabilities*, Phys. Rev. D 68 (2003) 033005 [hep-ph/0304056].
- [8] R.Tomas, M.Kachelrieß, G.Raelt, A.Dighe, H.-Th.Janka and L.Scheck, *Neutrino signatures of supernova shock and reverse shock propagation*, J. Cosmol. Astropart. Phys. JCAP 09 (2004) 015 [astro-ph/0407132].
- [9] G.L.Fogli, E.Lisi, A.Mirizzi and D.Montanino, *Probing supernova shock waves and neutrino flavor transitions in next-generation water-Cherenkov detectors*, J. Cosmol. Astropart. Phys. JCAP 04 (2005) 002 [hep-ph/0412046].
- [10] R.Buras, M.Rampp, H.-Th.Janka and K.Kifonidis, *Improved Models of Stellar Core Collapse and Still no Explosions: What is Missing?*, Phys. Rev. Lett. 90 (2003) 241101 [astro-ph/0303171].
- [11] R.Buras, M.Rampp, H.-Th.Janka and K.Kifonidis, *Two-dimensional hydrodynamic core-collapse supernova simulations with spectral neutrino transport. I. Numerical method and results for a 15 M_{sun} star*, astro-ph/0507135.
- [12] S.Goswami, A.Bandyopadhyay and S.Choubey, *Global analysis of neutrino oscillation*, Nucl. Phys. Proc. Suppl. 143 (2005) 121 [hep-ph/0409224].
- [13] A.B.Balanterkin, S.H.Fricke and P.J.Hatchell, *Analytical and semi-classical spectra of matter Enhanced Neutrino Oscillations*, Phys. Rev. D 38 (1988) 935.
- [14] L.Landau, *A theory of energy transfer II*, Phys. Z. Sowjetunion 2 (1932) 46.
- [15] C.Zener, *Nonadiabatic Crossing of Energy Levels*, Proc. Roy. Soc. Lond. A 137 (1932) 696.
- [16] A.S.Dighe, Q.Y.Liu and A.Yu.Smirnov, *Cohherence and the day-night asymmetry in the solar neutrino flux*, hep-ph/9903329.
- [17] T.K.Kuo and J.T.Pantaleone, Rev. Mod. Phys. 61 (1989) 937.
- [18] K.Nakamura, *Hyper-Kamiokande: A next generation water Cherenkov detector*, Int. J. Mod. Phys. A 18 (2003) 4053.
- [19] L.Oberauer, F.von Feilitzsch and W.Potzel, *A large liquid scintillator detector for low-energy neutrino astronomy*, Nucl. Phys. Proc. Suppl. 138 (2005) 108.
- [20] A.Bueno, I.Giulio Botella and A.Rubbia, *Supernova neutrino detection in a liquid argon TPC*, hep-ph/0307222.
- [21] R.Buras, H.-Th.Janka, M.T.Keil, G.G.Raelt and M.Rampp, *Electron-neutrino pair*

annihilation: A new source for muon and tau neutrinos in supernovae," *Astrophys. J.* 587 (2003) 320 [[astro-ph/0205006](#)].

[22] T. Totani, K. Sato, H. E. Dahl and J. R. Wilson, "Future detection of supernova neutrino burst and explosion mechanism," *Astrophys. J.* 496 (1998) 216 [[astro-ph/9710203](#)].

[23] A. S. Dighe, M. T. Keil and G. G. Raaf, "Identifying earth effects on supernova neutrinos at a single detector," *J. Cosmol. Astropart. Phys.* JCAP 06 (2003) 006 [[hep-ph/0304150](#)].

[24] A. S. Dighe, M. Kachelriess, G. G. Raaf and R. Tomas, "Signatures of supernova neutrino oscillations in the earth mantle and core," *J. Cosmol. Astropart. Phys.* JCAP 01 (2004) 004 [[hep-ph/0311172](#)].